

Interplay between Point and Extended Defects and Their Effects on Jerky Domain-Wall Motion in Ferroelectric Thin Films

Ralph Bulanadi^{1,*}, Kumara Cordero-Edwards¹, Philippe Tückmantel¹, Sahar Saremi², Giacomo Morpurgo¹, Qi Zhang³, Lane W. Martin^{2,4,5,6}, Valanoor Nagarajan³, and Patrycja Paruch¹

¹Department of Quantum Matter Physics, University of Geneva, 1211 Geneva, Switzerland

²Department of Materials Science and Engineering, University of California, Berkeley, California 94720, USA

³School of Materials Science and Engineering, University of New South Wales, Sydney, New South Wales 2052, Australia

⁴Materials Sciences Division, Lawrence Berkeley National Laboratory, Berkeley, California 94720, USA

⁵Departments of Materials Science and NanoEngineering, Chemistry, and Physics and Astronomy, Rice University, Houston, Texas 77005, USA

⁶Rice Advanced Materials Institute, Rice University, Houston, Texas 77005, USA

 (Received 23 November 2023; accepted 7 June 2024; published 5 September 2024)

Defects have a significant influence on the polarization and electromechanical properties of ferroelectric materials. Statistically, they can be seen as random pinning centers acting on an elastic manifold, slowing domain-wall propagation and raising the energy required to switch polarization. Here we show that the “dressing” of defects can lead to unprecedented control of domain-wall dynamics. We engineer defects of two different dimensionalities in ferroelectric oxide thin films—point defects externally induced via He²⁺ bombardment, and extended quasi-one-dimensional *a* domains formed in response to internal strains. The *a* domains act as extended strong pinning sites (as expected) imposing highly localized directional constraints. Surprisingly, the induced point defects in the He²⁺ bombarded samples orient and align to impose further directional pinning, screening the effect of *a* domains. This defect interplay produces more uniform and predictable domain-wall dynamics. Such engineered interactions between defects are crucial for advancements in ferroelectric devices.

DOI: [10.1103/PhysRevLett.133.106801](https://doi.org/10.1103/PhysRevLett.133.106801)

Ferroelectric oxides have long excited broad interest for both industrial applications in memory, sensing, and actuation [1–3], as well as fundamental physics, most recently with nontrivial, highly local polarization textures [4–8], and emergent functional properties at domain walls [9–11]. However, the observations and uses of ferroelectrics are invariably mediated by the defects ubiquitous to these materials, which can both inhibit and enhance desired properties [12–14]. Indeed, the intentional generation of defects has been used to stabilize the target multiferroic tetragonal-like phase of BaTiO₃ [15], control wake-up in HfO₂-based ferroelectrics [16,17] or enable novel properties like effective negative capacitance [18]. Defects induced through ion bombardment have been of particular interest in recent years, with ion-bombarded ferroelectric films showing increased resistivity [19], increased energy

density [20], or induced ferroelectricity in HfO₂-based films [21].

The plethora of potential properties and applications resulting from defect engineering should be of no surprise given the immense diversity of defects themselves [22–24]. Oxygen vacancies—point defects inevitable in oxide thin films—can be modulated via composition or growth conditions, and act both as pinning sites [25] and charge carriers [26,27]; features inexorably relevant to any ferroelectric application. In addition, phase boundaries and twins can introduce long-range strain effects, altering the continuity of polarization in their vicinity [28], and acting as extended defects (two-dimensional in bulk, quasi-one-dimensional in thin films) [29,30].

Despite this high diversity of defects in ferroelectric oxide thin films, properties emergent from their *interplay* remain as yet largely unexplored. In this Letter, we investigate the effects of an engineered, complex disorder landscape, including both point and extended defects, on the pinning and motion of ferroelectric domain walls during polarization switching under an applied electric field.

To minimize innate defect variations across samples, five PbTiO₃ films were simultaneously grown via pulsed laser deposition (PLD) on SrTiO₃ (001) substrates (CrysTec GmbH), with a 20 nm SrRuO₃ bottom electrode.

*Contact author: ralph.bulanadi@unige.ch

Published by the American Physical Society under the terms of the [Creative Commons Attribution 4.0 International license](https://creativecommons.org/licenses/by/4.0/). Further distribution of this work must maintain attribution to the author(s) and the published article's title, journal citation, and DOI.

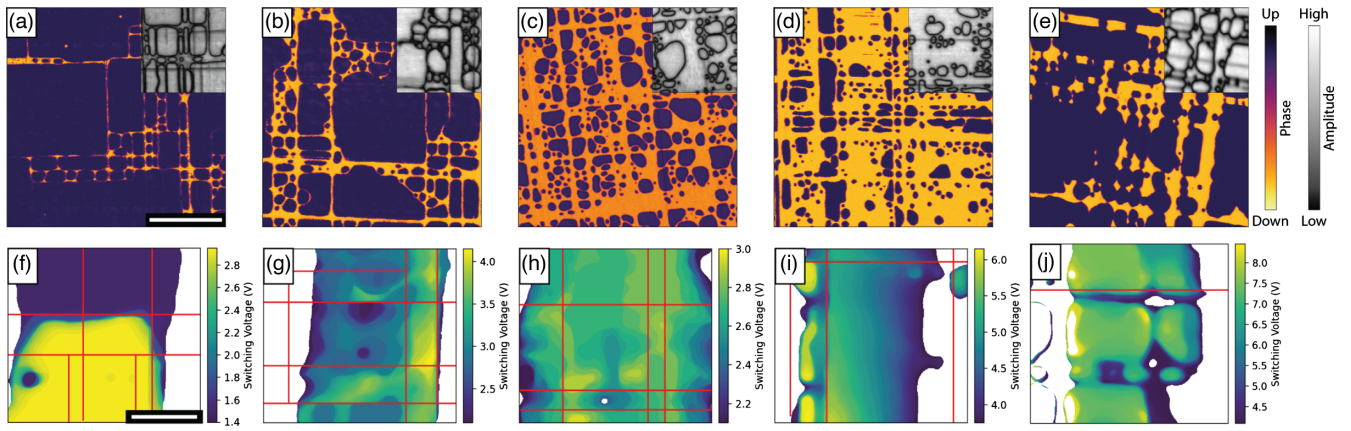


FIG. 1. Polarization switching studies in PbTiO_3 thin films. PFM phase imaging of the polarization state of (a) the as grown sample, as well as samples with He^+ bombardment densities of (b) 10^{13} , (c) 10^{14} , (d) 10^{15} , and (e) 10^{16} ions/ cm^2 . PFM amplitudes appear inset, corresponding to the regions overlaid. (f)–(j) Representative ferroelectric switching maps of corresponding samples. Color bars show the voltage needed to switch this region. The positions of the a domains are highlighted as red lines. Scale bars on the PFM images and switching maps mark $1\ \mu\text{m}$ and $500\ \text{nm}$, respectively.

As detailed in [19], the films were sufficiently thick (140 nm) for a domains to form during growth. To probe the effects of increasing point defect concentration, four samples were bombarded by He^{2+} ions with an energy of 5 MeV, at flux densities of 10^{13} , 10^{14} , 10^{15} , and 10^{16} ions/ cm^2 (this bombardment energy was chosen to be sufficiently high for the ions to penetrate entirely through the film and stop within the substrate). One sample was maintained in its pristine as-grown state, so that the only defects present were those formed during growth. High crystalline quality and out-of-plane c -axis orientation in all samples were verified by x-ray diffraction, with reciprocal space maps around the (002)-diffraction peak revealing the presence of a -axis-oriented twin domains (Fig. S1 in the Supplemental Material [31]). Diffraction peak positions were comparable among all samples, but the full width at half maximum of the film diffraction peak gradually increased with increasing ion bombardment (Fig. S2 in [31]). This suggests that the He^{2+} ions are not themselves injected into the sample [38], but rather cause radiation damage and the formation of complex defect clusters [19].

A majority c -phase of PbTiO_3 was identified via piezoresponse force microscopy (PFM) [Figs. 1(a)–1(e)]. Both up- and down-oriented c domains were observed, marked by a 180° phase shift (Fig. S3 in [31]), with their relative proportion varying significantly with He^{2+} bombardment density. The pristine sample showed a predominantly up-orientated polarization, with small down-oriented domains preferentially segregating at the a -domain network. The volume of these down domains increased with He^{2+} bombardment density to become the dominant orientation. However, at the highest bombardment density, we observed a return to the majority up-polarization orientation. The a domains were observed in all samples as sparse, irregular grids, aligned with the in-plane axes and

marked by a drop in the out-of-plane amplitude without a corresponding phase shift.

To track domain-wall motion in a controlled configuration [Figs. 1(f)–1(j)], a vertical stripe domain was first patterned using a biased scanning probe microscopy tip. Once the domain wall position stabilised and relaxed (Fig. S3 in [31]), a gradual polarization reversal was then carried out by stroboscopic measurements: switching scans with a defined dc bias were interleaved with PFM scans to image the evolution of the domain-wall position, with the bias gradually incremented between cycles by a fixed interval of 50 mV. This stroboscopic switch–image cycling proceeded until either complete polarization reversal or until no further evolution of the domain configuration was observed over at least five cycles. The evolution of both up- and down-oriented stripe domains were examined, with each measurement repeated 2–3 times on different regions of each sample.

Ferroelectric switching in each sample appears qualitatively distinct [Figs. 1(f)–1(j)]. In the pristine sample, we observe the abrupt reversal of relatively large areas, whose boundaries correlate strongly with the presence of the a domains. With increasing He^{2+} bombardment flux density, polarization reversal is generally slower—significantly so for the highest bombardment densities—and proceeds more gradually via smaller switching steps, suggesting increased pinning effects less correlated with the a -domain positions.

The global effects of He^{2+} bombardment can be more quantitatively gauged by measuring the evolution of polarization reversal [Fig. 2(a)], calculated as the ratio of the area switched through the stroboscopic switching scans, compared to the area of the initially patterned stripe. The pristine films present a slight negative imprint: the onset of switching (~ 1.50 V) and the coercive voltage V_P (~ 2.75 V, where 50% polarization reversal occurred) were

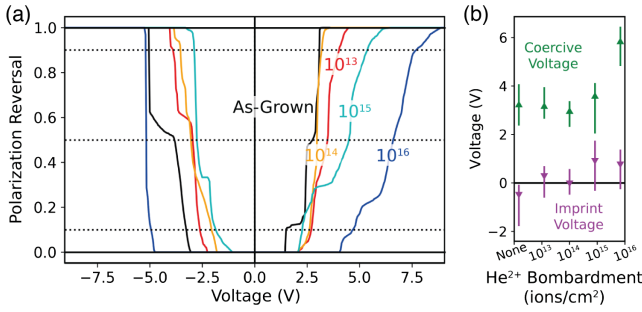


FIG. 2. Switching dynamics in PbTiO_3 thin films under incrementally increasing voltage. (a) Polarization reversal as a function of applied voltage, averaged over 2–3 experiments. Dashed lines represent 10%, 50%, and 90% reversal. Inscribed values mark He^{2+} bombardment levels in ions/cm^2 . (b) Corresponding switching characteristics, with average coercive voltage $V_C = [(|V_P| + |V_N|)/2]$ and imprint $V_I = [(|V_P| - |V_N|)/2]$. Markers denote the V_P and V_N for which 50% polarization reversal was observed, while error bars span the voltage range between 10% and 90% polarization reversal.

lower magnitude under positive tip biases than the onset and coercive voltage (V_N , defined analogously) under negative tip biases (~ -3.25 and ~ -3.5 V, respectively). Low bombardment densities, up to about 10^{15} ions/cm^2 , slightly decrease the magnitude of V_N and increases V_P , potentially making the imprint more positive and the overall switching response more symmetric [Fig. 2(b)]. The coercive voltages did not appear to significantly change with bombardment level.

With yet increasing bombardment densities, however, the effects on switching become more dramatic, with both positive and negative coercive voltages significantly increased. As expected given the charged nature of the bombarding ions, these effects are themselves highly asymmetric [39], potentially further increasing the imprint by extending the range of voltages over which switching occurs under positive tip bias, while switching under negative tip bias is rendered even more abrupt. These

direct, nanoscale measurements also support prior work by Saremi *et al.* that similarly show dramatic changes of the ferroelectric switching loops only above 10^{15} ions/cm^2 [40]. These observations of the global switching dynamics are further corroborated by switching spectroscopy PFM measurements (Fig. S4 in [31]).

To ascertain the *dynamics* of the ferroelectric switching, we look to the distribution of sizes of switching events, with a particular interest in ultraslow creep dynamics occurring for highly subcritical electric fields [32,41]. Ferroelectric switching dynamics are known to follow a highly stable, scale-invariant power law, where the logarithm of the probability of a switching “event” occurring decreases linearly with the logarithm of the magnitude of the area reoriented, or the energy released by this reorientation [32,42–48]. Changes in this global power-law distribution would therefore indicate changes to the underlying switching mechanism resulting from modifications to the disorder landscape. Individual switching events are therefore extracted from the switching maps of each measurement series, such as those shown in Figs. 1(f)–1(j), using the procedure detailed in Supplemental Material, Sec. III [31].

We observe power-law scaling of event sizes in all five samples [Fig. 3(a)]. The estimated scaling parameter $\hat{\alpha}$ was identified through maximum-likelihood methods, following Clauset *et al.* [33], and described in Fig. 1(j), using the procedure detailed in Supplemental Material, Sec. III [31]. In brief, the y axis marks the exponent calculated to be maximally likely, as a function of a cutoff at which all lower values are ignored and excluded. With low magnitude cutoffs, we are vulnerable to random noise in measurement, while with high magnitude cutoffs we eliminate relevant data. In all five samples, however, $\hat{\alpha} \sim 2.0$ over approximately 2 orders of magnitude of the magnitude cutoff.

This consistency in the estimated critical exponent is remarkable given the qualitative differences in switching maps between the different samples [Figs. 1(f)–1(j)]. Moreover, one could expect that the increased defects in

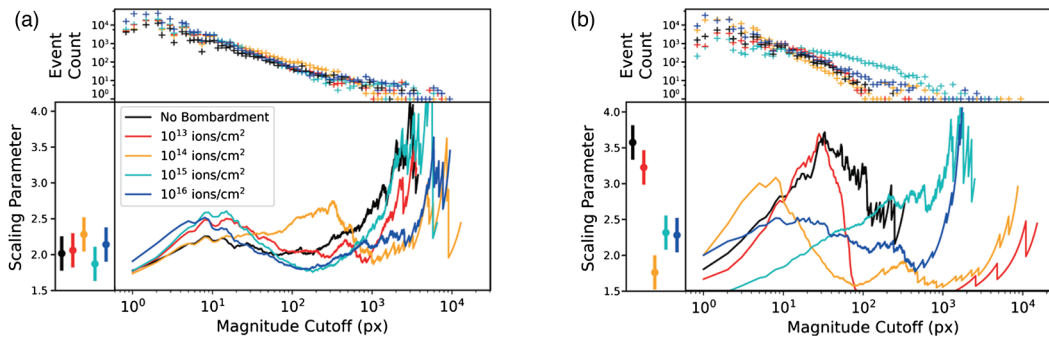


FIG. 3. Power-law fits of ferroelectric switching dynamics, under (a) incrementally increasing voltage and (b) constant voltage. Top panels: Log-log plots of the distribution of switching event size. Center panels: Optimal power-law scaling parameters for different event-size cutoffs calculated via maximum-likelihood estimation. Left panels: The scaling parameter corresponding to minimum Kolmogorov-Smirnov statistic. Error bars use a root-mean-squared error of 0.2 as expected for this method of domain-wall extraction [49].

the most bombarded samples may increase conduction or leakage [22], and thus alter the distribution of switching events. Despite this, the similarity of the final critical exponent indicates that all samples show similar crackling behavior. These experimental observations are also exceptionally consistent: the stability of the critical exponent over 2 orders of magnitude on the plot of maximum-likelihood exponents is particularly extensive given the inevitable noise and size constraints of real data [33].

We note that this analysis is based on the full dataset of all switching events, including the largest ones occurring at the highest tip bias. As previously reported by Tückmantel *et al.* [32], these large events may indicate a combination of creep and depinning regimes which could depress the value of the power-law scaling exponent. We therefore performed a further investigation of switching dynamics at constant tip bias well below the coercive voltage determined for each sample from Fig. 2. Specifically, we used 1 V for the samples bombarded with 10^{13} and 10^{14} ions/cm², as well as the non-ion-bombarded sample, and 1.5 V for the sample bombarded with 10^{15} and 10^{16} ions/cm², carrying out three independent stroboscopic switching–imaging experiments in each sample.

The scaling parameters are far less stable for these constant-voltage studies [Fig. 3(b)]. This is particularly true for the as-grown (non-ion-bombarded) and lowest-bombardment density samples, where the high values obtained for the scaling parameter (above 3) could be a marker for non-power-law behavior [49]. This may be related to the switching voltage magnitude: for these samples, in particular, switching proceeded at a rapid enough rate that statistics were insufficient for an adequate power-law fit. However, at lower biases, no significant domain-wall motion could be observed within a reasonable timeframe. This trend is akin to those seen in Fig. 2(a), where polarization switching in these samples proceeds over a smaller threshold. In the higher-bombardment-density samples, the scaling parameter appears physically meaningful, but smaller events play a more significant role,

and increase the measured value to closer to 2.5, consistent with previous observations in the creep regime [32].

In both analyses, we find that the bombardment density has only weak effects on the value of the scaling parameter $\hat{\alpha}$, which varies between 1.8 and 2.3 for the incrementally increased tip bias measurements, and between 1.9 and 2.4 for the constant tip bias measurements. The consistency of the scaling exponent across samples further suggests that (a) the creep regime dominates the switching dynamics in these samples, and (b) the pinning effects stay in the same universality class, regardless of defect density.

At a local, rather than global level, however, the effects of the a domains can be quite significant; this can be seen qualitatively in Figs. 1(f)–1(j), where much of the pinning appears in the vicinity of—and parallel to—nearby a domains. To better understand their role in conjunction with the bombardment-induced point defects, we therefore focus on local variations in domain-wall dynamics. This analysis is again based on the domain switching maps, of which a subset is shown in Figs. 1(f)–1(j). As before, the positions of the a domains are individually tracked, and each switching map is interpolated to obtain a smooth and continuously varying representation of the switching voltage across the ferroelectric surface.

One such interpolated switching map, obtained on the pristine sample and projected into three dimensions, is shown in Fig. 4(a), with a domains indicated in red. Parallel to the a_1 domain and ~ 100 nm away from it, a rapid increase in the magnitude of the switching voltage can be seen. This increase corresponds physically to an abrupt and marked increase in switching difficulty, and thus higher pinning than in the surrounding regions. This observation is even clearer after taking a spatial derivative in the a_1 direction [Fig. 4(b)], where high values of the derivative appear parallel to the a_1 domain, clearly indicating the strong domain-walls pinning in this region.

A line profile of the average height of the derivative along the a_1 direction is shown in Fig. 4(c). We observe a distinct

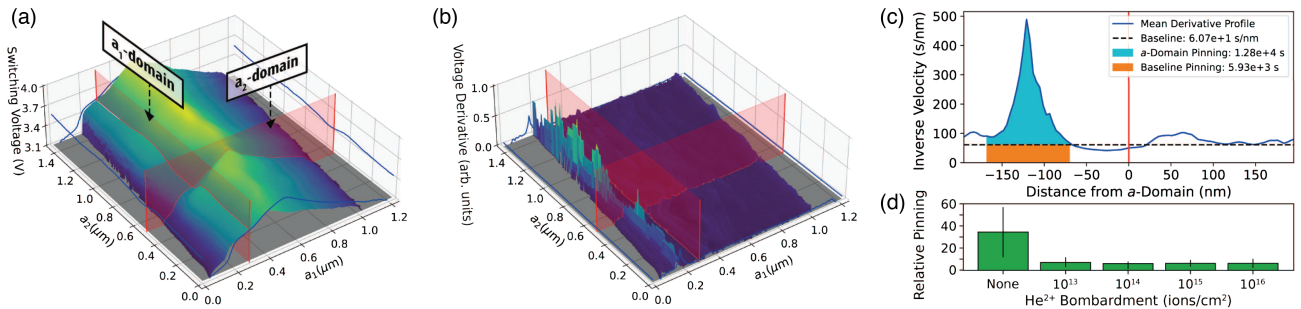


FIG. 4. Extraction of the pinning contribution of quasi-one-dimensional a domains. (a) Interpolated switching map of the non-ion-bombarded PbTiO₃ thin film, projected into three dimensions. Red lines mark the positions of a domains at the ferroelectric surface. Blue lines show the switching voltage profile averaged along the a_1 and a_2 crystalline axes. (b) Normalized a_1 derivative of the switching map. (c) Line profile of the a_1 spatial derivative in the vicinity of the a_1 domain (marked in a red solid line). The dashed black line corresponds to the average derivative value in the switching map after neglecting events in the vicinity of a domains. A peak in the derivative and pinning is highlighted in cyan, with the area beneath it corresponding to the average pinning, marked in orange. (d) A column plot comparing the ratio of the pinning attributed to the a domains to the pinning attributed to the baseline for all samples.

peak, which we believe corresponds to the pinning effect of the a domain. The pinning strength, indicated by the dashed line, is far above the baseline level of the sample. This analysis therefore allows us to distinguish two regions with qualitatively different contributions; a low-level *baseline* pinning which corresponds to behavior consistent throughout the entire sample, and an a -domain contribution identifiable in the line profile by a sharp peak in the vicinity of an a domain. Plots of these respective contributions across the samples (Fig. S5 in [31]), show both increasing after He^{2+} bombardment. The ratio between the two, however, shows a vastly different trend [Fig. 4(d)], where the pristine (non-bombarded) sample presents a uniquely higher pinning contribution from the a domains as compared to the baseline.

Under as-grown conditions, therefore, the a domains have significant local contributions to the pinning, which in turn carries heavy implications for the global pinning and power-law scaling. As a significant portion of small domain-wall motion events occurs in the direct vicinity of a domains (particularly in the as-grown sample), we conclude that these extended quasi-one-dimensional defects contribute to an increase in the value of the scaling parameter measured across the whole sample. Indeed, in similar thin films of the related material $\text{Pb}(\text{Zr}_{0.2}\text{Ti}_{0.8})\text{O}_3$ without a domains, lower values of the global scaling parameter were observed in the creep regime [32].

However, quite different domain-wall interactions emerge in the bombarded samples, where the relative difference between the baseline pinning and a -domain contribution is nowhere near so significant. Specifically, at any level of He^{2+} bombardment we see a marked increase in baseline pinning [Fig. S5(b) in [31]]. Rather than being strongly pinned only at the a domains, the domain walls in these samples are subject to comparable variations throughout the entire potential energy landscape. Effectively, the bombardment defects can be seen as “dressing” the strong confinement effects of the a domains, which are reflected in the corresponding decrease in the value of the scaling parameter.

This dressing of a domains after any ion bombardment may appear to contrast with Fig. 2 and Ref. [40], where significant variations in switching voltage are observed only with bombardment above 10^{15} ions/cm²; and with as Fig. 3(a), where similar scaling parameters are observed across all samples. How can similar distributions of event sizes be observed in both the as-grown sample with strong, highly directional pinning by a domains, and in the ion-bombarded samples with an increased but not presumably directional collective pinning due to the He^{2+} ions?

This answer is revealed by the switching maps themselves [Figs. 1(f)–1(j)]. In the most bombarded sample [Fig. 1(j)], significant pinning appears parallel to the crystallographic axes, but far removed from any observed a domains. These regions act akin to the a domains and contribute to a similar distribution of small and large events among all samples.

Likewise, while the switching voltages may change, these changes need not impact switching event size.

As to the nature of these regions, we note that the identical and simultaneous growth of these thin films minimizes potential variations between them. Rather, the only notable difference between these samples is the increasing level of He^{2+} bombardment and the resulting point-defect density, which must therefore selectively segregate or orient along the crystallographic axes.

Indeed, previous simulations actually suggest that aligned point defects may have strikingly similar pinning effects to those of a domains. Kimmel *et al.* used *ab initio* calculations to show that oxygen vacancies prefer c -axis sites over a -axis sites, and this preference can drive the rotation of the entire unit cell around the vacancy [50]. In our case, defects induced by He^{2+} ion bombardment could be a preferential site for oxygen vacancy colocalization, and thus drive such axial rotations, resulting in the formation of features acting akin to a domains, with associated directional pinning in the bombarded samples.

The implications of this screening of a -domain pinning by point defects are twofold. First, our Letter suggests that the key to more controllable ferroelectric switching may not be more perfect, less-defective films, but indeed the opposite, with induced defects ensuring more consistent switching dynamics. Meanwhile, at the nanoscale, the inferred organization of point-defects along crystallographic axes could potentially lead to the formation and stabilization of new polarization textures.

In summary, we investigated the interplay between extended quasi-one-dimensional (a domain) and point (He^{2+} bombardment and implantation) defects, and their effects on ferroelectric switching and domain-wall motion. We found more intense He^{2+} bombardment associated with an increase in coercive voltage. Despite the subsequent increase in driving voltages required, all samples maintained a power-law distribution of switching event size dominated by creep dynamics, with critical exponent values highly stable both within an individual experiment and across samples that had undergone different levels of He^{2+} bombardment. We simultaneously observed a remarkable local-scale interaction between the bombardment defects and the a -domains, where the point defects appear to dress the extended defects, effectively screening their pinning strength. Such additional point defects can thus induce more uniform and predictable domain-wall dynamics. Moreover, at increasing He^{2+} bombardment densities, the point defects themselves appear to segregate and align with the crystalline axes of the ferroelectric, giving rise to directional pinning more evenly distributed through the sample. This understanding of the effects of a domains and point defects on ferroelectric switching dynamics and scaling parameters can therefore help to further enhance ferroelectric device performance via defect engineering.

Acknowledgments—This work was supported by the Swiss National Science Foundation under Division II (Grant No. 200021-178782). G. M. acknowledges additional support from the Swiss National Science Foundation under Grant No. 2000020-188687. S. S. acknowledges support from the National Science Foundation under Grant No. DMR-2102895. L. W. M. acknowledges support from the Army Research Office under Grant No. W911NF-21-1-0118. The research at UNSW is supported by the Australian Research Council Centre of Excellence in Future Low-Energy Electronics Technologies (Project No. CE170100039).

Data availability—The data that support the findings of this study are available on Yareta [51].

R. B. performed the PFM and x-ray diffraction measurements, and carried out the analysis. S. S. grew the films. K. C. E., P. T., and G. M. performed preliminary analysis. The manuscript was written by R. B. and P. P. Q. Z., L. W. M., N. V., and P. P. supervised the project. All authors contributed to the scientific discussion and manuscript revisions.

-
- [1] P. Muralt, Ferroelectric thin films for micro-sensors and actuators: A review, *J. Micromech. Microeng.* **10**, 136 (2000).
- [2] P. Lopez-Varo *et al.*, Physical aspects of ferroelectric semiconductors for photovoltaic solar energy conversion, *Phys. Rep.* **653**, 1 (2016).
- [3] J. F. Scott and C. A. P. De Araujo, Ferroelectric memories, *Science* **246**, 1400 (1989).
- [4] A. Yadav *et al.*, Observation of polar vortices in oxide superlattices, *Nature (London)* **530**, 198 (2016).
- [5] I. I. Naumov, L. Bellaïche, and H. Fu, Unusual phase transitions in ferroelectric nanodisks and nanorods, *Nature (London)* **432**, 737 (2004).
- [6] C.-L. Jia, K. W. Urban, M. Alexe, D. Hesse, and I. Vrejoiu, Direct observation of continuous electric dipole rotation in flux-closure domains in ferroelectric Pb(Zr, Ti)O₃, *Science* **331**, 1420 (2011).
- [7] S. Das *et al.*, Observation of room-temperature polar skyrmions, *Nature (London)* **568**, 368 (2019).
- [8] B.-K. Lai, I. Ponomareva, I. I. Naumov, I. Kornev, H. Fu, L. Bellaïche, and G. J. Salamo, Electric-field-induced domain evolution in ferroelectric ultrathin films, *Phys. Rev. Lett.* **96**, 137602 (2006).
- [9] G. Catalan, J. Seidel, R. Ramesh, and J. F. Scott, Domain wall nanoelectronics, *Rev. Mod. Phys.* **84**, 119 (2012).
- [10] D. Meier, Functional domain walls in multiferroics, *J. Phys. Condens. Matter* **27**, 463003 (2015).
- [11] E. K. Salje, Multiferroic domain boundaries as active memory devices: Trajectories towards domain boundary engineering, *ChemPhysChem* **11**, 940 (2010).
- [12] D. Damjanovic, Hysteresis in piezoelectric and ferroelectric materials, in *Science of Hysteresis* (2006), ISBN 0-12-480874-3.
- [13] Y. Feng, J. Wu, Q. Chi, W. Li, Y. Yu, and W. Fei, Defects and aliovalent doping engineering in electroceramics, *Chem. Rev.* **120**, 1710 (2020).
- [14] W. Dong *et al.*, Engineering the defects and microstructures in ferroelectrics for enhanced/novel properties: An emerging way to cope with energy crisis and environmental pollution, *Adv. Sci.* **9**, 2105368 (2022).
- [15] D. Sando, T. Young, R. Bulanadi, X. Cheng, Y. Zhou, M. Weyland, P. Munroe, and V. Nagarajan, Designer defect stabilization of the super tetragonal phase in > 70-nm-thick BiFeO₃ films on LaAlO₃ substrates, *Jpn. J. Appl. Phys.* **57**, 0902B2 (2018).
- [16] A. Kashir, S. Oh, and H. Hwang, Defect engineering to achieve wake-up free HfO₂-based ferroelectrics, *Adv. Eng. Mater.* **23**, 2000791 (2021).
- [17] B. Noheda, P. Nukala, and M. Acuautila, Lessons from hafnium dioxide-based ferroelectrics, *Nat. Mater.* **22**, 562 (2023).
- [18] P. Zubko, J. C. Wojdeł, M. Hadjimichael, S. Fernandez-Pena, A. Sené, I. Luk'yanchuk, J.-M. Triscone, and J. Íñiguez, Negative capacitance in multidomain ferroelectric superlattices, *Nature (London)* **534**, 524 (2016).
- [19] S. Saremi, R. Xu, L. R. Dedon, J. A. Mundy, S.-L. Hsu, Z. Chen, A. R. Damodaran, S. P. Chapman, J. T. Evans, and L. W. Martin, Enhanced electrical resistivity and properties via ion bombardment of ferroelectric thin films, *Adv. Mater.* **28**, 10750 (2016).
- [20] J. Kim, S. Saremi, M. Acharya, G. Velarde, E. Parsonnet, P. Donahue, A. Qualls, D. Garcia, and L. W. Martin, Ultrahigh capacitive energy density in ion-bombarded relaxor ferroelectric films, *Science* **369**, 81 (2020).
- [21] S. Kang *et al.*, Highly enhanced ferroelectricity in HfO₂-based ferroelectric thin film by light ion bombardment, *Science* **376**, 731 (2022).
- [22] S. Aggarwal and R. Ramesh, Point defect chemistry of metal oxide heterostructures, *Annu. Rev. Mater. Sci.* **28**, 463 (1998).
- [23] S. V. Kalinin, S. Jesse, A. Tselev, A. P. Baddorf, and N. Balke, The role of electrochemical phenomena in scanning probe microscopy of ferroelectric thin films, *ACS Nano* **5**, 5683 (2011).
- [24] D. M. Evans *et al.*, Conductivity control via minimally invasive anti-Frenkel defects in a functional oxide, *Nat. Mater.* **19**, 1195 (2020).
- [25] S. Jesse *et al.*, Direct imaging of the spatial and energy distribution of nucleation centres in ferroelectric materials, *Nat. Mater.* **7**, 209 (2008).
- [26] M. Raymond and D. Smyth, Defects and charge transport in perovskite ferroelectrics, *J. Phys. Chem. Solids* **57**, 1507 (1996).
- [27] A. Pramanick, A. D. Prewitt, J. S. Forrester, and J. L. Jones, Domains, domain walls and defects in perovskite ferroelectric oxides: A review of present understanding and recent contributions, *Crit. Rev. Solid State Mater. Sci.* **37**, 243 (2012).
- [28] C. Stefani, L. Ponet, K. Shapovalov, P. Chen, E. Langenberg, D. G. Schlom, S. Artyukhin, M. Stengel, N. Domingo, and G. Catalan, Mechanical softness of ferroelectric 180° domain walls, *Phys. Rev. X* **10**, 041001 (2020).

- [29] L. Puntigam, M. Althaler, S. Ghara, L. Prodan, V. Tsurkan, S. Krohns, I. Kézsmárki, and D. M. Evans, Strain driven conducting domain walls in a Mott insulator, *Adv. Electron. Mater.* **8**, 2200366 (2022).
- [30] E. K. Salje and X. Ding, Ferroelastic domain boundary-based multiferroicity, *Crystals* **6**, 163 (2016).
- [31] See Supplemental Material at <http://link.aps.org/supplemental/10.1103/PhysRevLett.133.106801>, which includes Refs. [32–37], for additional detail regarding experimental and analysis methods.
- [32] P. Tückmantel, I. Gaponenko, N. Caballero, J. C. Agar, L. W. Martin, T. Giamarchi, and P. Paruch, Local probe comparison of ferroelectric switching event statistics in the creep and depinning regimes in $\text{Pb}(\text{Zr}_{0.2}\text{Ti}_{0.8})\text{O}_3$ thin films, *Phys. Rev. Lett.* **126**, 117601 (2021).
- [33] A. Clauset, C. R. Shalizi, and M. E. Newman, Power-law distributions in empirical data, *SIAM Rev.* **51**, 661 (2009).
- [34] S. Jesse, A. P. Baddorf, and S. V. Kalinin, Switching spectroscopy piezoresponse force microscopy of ferroelectric materials, *Appl. Phys. Lett.* **88**, 062908 (2006).
- [35] E. N. Mortensen and W. A. Barrett, Morphological interpolation between contour lines, in *Medical Imaging 1993: Image Processing* (International Society for Optics and Photonics, 1993), Vol. 1898, pp. 501–510, [10.1117/12.154537](https://doi.org/10.1117/12.154537).
- [36] L. Musy, R. Bulanadi, I. Gaponenko, and P. Paruch, Hystorian: A processing tool for scanning probe microscopy and other n-dimensional dataset, *Ultramicroscopy* **228**, 113345 (2021).
- [37] E. K. H. Salje, A. Planes, and E. Vives, Analysis of crackling noise using the maximum-likelihood method: Power-law mixing and exponential damping, *Phys. Rev. E* **96**, 042122 (2017).
- [38] H. Guo *et al.*, Strain doping: Reversible single-axis control of a complex oxide lattice via helium implantation, *Phys. Rev. Lett.* **114**, 256801 (2015).
- [39] E. D. Roede, A. B. Mosberg, D. M. Evans, E. Bourret, Z. Yan, A. T. J. van Helvoort, and D. Meier, Contact-free reversible switching of improper ferroelectric domains by electron and ion irradiation, *APL Mater.* **9**, 021105 (2021).
- [40] S. Saremi, J. Kim, A. Ghosh, D. Meyers, and L. W. Martin, Defect-induced (dis) order in relaxor ferroelectric thin films, *Phys. Rev. Lett.* **123**, 207602 (2019).
- [41] P. Paruch and J. Guyonnet, Nanoscale studies of ferroelectric domain walls as pinned elastic interfaces, *C.R. Phys.* **14**, 667 (2013).
- [42] J. P. Sethna, K. A. Dahmen, and C. R. Myers, Crackling noise, *Nature (London)* **410**, 242 (2001).
- [43] N. Friedman, A. T. Jennings, G. Tsekenis, J. Y. Kim, M. Tao, J. T. Uhl, J. R. Greer, and K. A. Dahmen, Statistics of dislocation slip avalanches in nanosized single crystals show tuned critical behavior predicted by a simple mean field model, *Phys. Rev. Lett.* **109**, 095507 (2012).
- [44] E. K. Salje and K. A. Dahmen, Crackling noise in disordered materials, *Annu. Rev. Condens. Matter Phys.* **5**, 233 (2014).
- [45] E. K. H. Salje, D. Xue, X. K. A. Ding, Dahmen, and J. Scott, Ferroelectric switching and scale invariant avalanches in BaTiO_3 , *Phys. Rev. Mater.* **3**, 014415 (2019).
- [46] C. Tan, C. Flannigan, J. Gardner, F. D. Morrison, E. K. H. Salje, and J. F. Scott, Electrical studies of Barkhausen switching noise in ferroelectric PZT: Critical exponents and temperature dependence, *Phys. Rev. Mater.* **3**, 034402 (2019).
- [47] B. Casals, G. F. Nataf, D. Pesquera, and E. K. Salje, Avalanches from charged domain wall motion in BaTiO_3 during ferroelectric switching, *APL Mater.* **8**, 011105 (2020).
- [48] T. Tybell, P. Paruch, T. Giamarchi, and J.-M. Triscone, Domain wall creep in epitaxial ferroelectric $\text{Pb}(\text{Zr}_{0.2}\text{Ti}_{0.8})\text{O}_3$ thin films, *Phys. Rev. Lett.* **89**, 097601 (2002).
- [49] R. Bulanadi and P. Paruch, Identifying and analyzing power-law scaling in two-dimensional image datasets, *Phys. Rev. E* **109**, 064135 (2024).
- [50] A. V. Kimmel, P. M. Weaver, M. G. Cain, and P. V. Sushko, Defect-mediated lattice relaxation and domain stability in ferroelectric oxides, *Phys. Rev. Lett.* **109**, 117601 (2012).
- [51] R. Bulanadi, Yareta, [10.26037/yareta:sqti2pvttnak3f6qoyql-pu6mc4](https://doi.org/10.26037/yareta:sqti2pvttnak3f6qoyql-pu6mc4).